ELSEVIER

Marine and Petroleum Geology 19 (2002) 307–322

Marine and Petroleum Geology

www.elsevier.com/locate/marpetgeo

Saline groundwater in the Münsterland Cretaceous Basin, Germany: clues to its origin and evolution

Matthias Grobe[a,*], Hans G. Machel[b]

[a]*Alberta Energy and Utilities Board, Alberta Geological Survey, 4th Floor Twin Atria Building, 4999-98 Ave, Edmonton, Alta., Canada T6B 2X3*
[b]*Department of Earth and Atmospheric Sciences, University of Alberta, Edmonton, Alta., Canada*

Received 15 January 2001; received in revised form 20 May 2001; accepted 10 June 2001

Abstract

Saline groundwater (TDS up to 250,000 mg/l) occurs in subsurface coal mines, wells, and artesian springs in the area of the halite-free Münsterland Cretaceous Basin (MCB) in Germany. The origin and evolution of the saline groundwater in the MCB are poorly understood. An investigation of the hydrochemistry and stable isotope (O, H, Sr) composition of a small sample set of present-day saline groundwater from the MCB has been carried out to improve our understanding of its origin and evolution within the framework of the complex geological history of the area.

The data provide evidence for: (1) halite dissolution, (2) water–rock interaction of highly saline fluids with siliciclastic sediments, (3) mixing of highly saline fluids with less saline waters of marine isotopic composition, (4) fault-controlled upward movement of warm saline ^{87}Sr-enriched groundwater from the Paleozoic bedrock into the overlying Late Cretaceous limestone aquifer, (5) water–rock interaction of ascending saline groundwater with the limestone aquifer, and (6) dilution by meteoric water. For the investigated sample set, the subrecent processes of mixing of different saline groundwaters, water–rock interaction, and dilution by modern meteoric water are volumetrically predominant, so that inferences about the early groundwater-forming processes have to rely mainly on our present understanding of the geological history of the area.

The results of this study have a bearing on questions related to the timing and origin of Pb–Zn and strontianite mineralizations within and in the periphery of the MCB, and are of direct interest to the small, but vibrant, salt-water spa industry in the area.

Keywords: Basinal brines; Fluid origin; Fluid evolution; Stable isotopes; Hydrochemistry; Water–rock interaction; Fluid mixing

1. Introduction

1.1. Background

The term groundwater, as used herein, refers to all aqueous subsurface fluids that occur beneath the water table in soils and geologic formations that are fully saturated (Freeze & Cherry, 1979). In this paper, the term *saline groundwater* refers to all groundwater with salinity (= total dissolved solids or TDS) higher than that of freshwater (TDS > 1000 mg/l) (Solley, 1983) and includes the salinity ranges of brackish water (TDS = 1000–10,000 mg/l), saline water (TDS = 10,000–100,000 mg/l), and brine water (TDS > 100,000 mg/l) (Carpenter, 1978).

A major physical attribute of most saline groundwaters is that they have migrated over long distances prior to entering the reservoir rocks or aquifers from where they presently reside and from which they can be produced. In many instances, significant chemical reactions between waters and minerals seem to have occurred elsewhere in the subsurface and, hence, the chemical compositions of the waters often bear little or no relation to the mineralogical framework of the present reservoir rocks or aquifers (Chaudhuri & Clauer, 1993). Furthermore, it is widely recognized that saline groundwaters play an important role in processes such as hydrocarbon migration, subsurface dolomitization, and the formation of sediment-hosted ore deposits (Bethke & Marshak, 1990; Kesler et al., 1997; Morrow, 1998; Sverjensky, 1984), but the origin(s) and source(s) of the water and solutes remain controversial. Saline groundwaters may originate as meteoric water that percolates into the subsurface and reacts with rocks along its path; or as interstitial seawater (connate water) trapped during original sediment deposition (Lowry, Faure, Mullet, & Jones, 1988). Subsequent chemical and isotopic changes may result

* Corresponding author. Fax: +1-780-422-2728.
E-mail address: matt.grobe@gov.ab.ca (M. Grobe).

0264-8172/02/$ - see front matter
PII: S0264-8172(02)00019-3

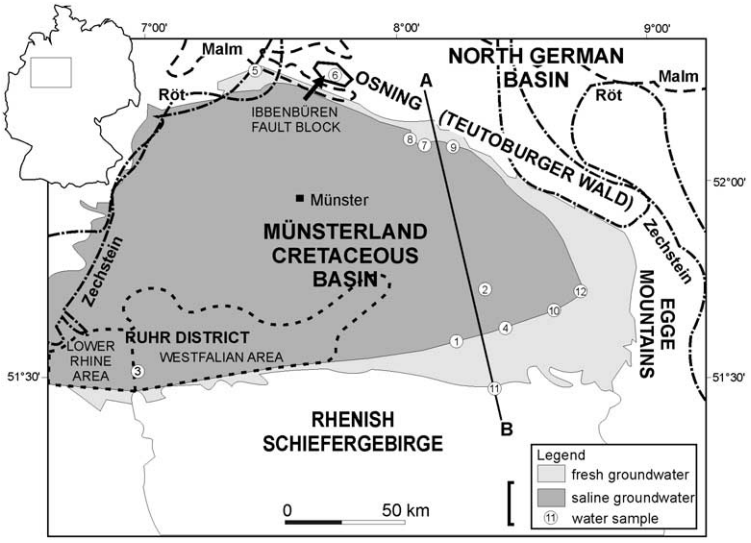

Fig. 1. Map of the MCB in northwestern Germany showing the distribution of saline groundwater (TDS > 1000 mg/l) in the regional aquifer. Dashed lines labeled Zechstein, Röt, and Malm delineate the southernmost extent of Upper Permian, Triassic, and Jurassic halite deposits in the subsurface (modified after Michel (1983a)). Solid line A–B indicates position of a schematic cross-section shown in Fig. 3.

from: (1) dilution of the saline groundwater by meteoric water; (2) migration and mixing of different saline groundwaters with contrasting chemical and isotopic compositions; and (3) water–rock interaction. The salinity of the groundwaters has been attributed to halite dissolution (Land & Prezbindowski, 1981), retention or reflux of evaporatively concentrated seawater (Carpenter, 1978; Rittenhouse, 1967), shale membrane filtration (Graf, 1982), and/or evaporation of non-marine fluids (Hardie, 1990).

The compositions and distribution of saline groundwater (TDS up to 250,000 mg/l) in subsurface coal mines, wells, and artesian springs in the area of the halite-free Münsterland Cretaceous Basin (MCB) in Germany have been the subject of numerous publications in the past 50 years (Angerer, Michel, & Semmler, 1968; Fricke, 1961, 1963, 1964a,b, 1967, 1968, 1969; Fricke & Wevelmeyer, 1960; Geyh & Michel, 1974; Michel, 1963; Michel & Nielsen, 1977; Patteisky, 1954; Puchelt, 1964; Wedewardt, 1995). Several theories about their origin(s) exist. Patteisky (1954) proposed a magmatic origin of the saline waters as so-called juvenile water. Puchelt (1964) suggested that the saline groundwaters are derived from the primary sedimentary pore waters (connate water) that underwent compositional modifications due to water–rock interaction and biological activity (e.g. sulfate reducing bacteria), whereas Fricke (1961) and Michel and Nielsen (1977) invoked the subsurface dissolution (subrosion) of halite deposits in the periphery of the MCB and migration of the resulting brines into the basin. Most recent publications (Michel, 1983a,b, 1994; Michel, Rabitz, & Werner, 1974; Wedewardt, 1995) conclude that the present-day compositions of the saline groundwaters in the MCB are a result of the complex hydrogeologic history of the area that led to the mixing of fluids of different origins (modified sedimentary pore water, subrosion brines, meteoric water).

The main objective of the present study is to better delineate the origin(s) and evolution of the saline groundwaters in the MCB within the framework of its complex geological history using oxygen, hydrogen, and strontium isotopes in conjunction with their chemical compositions. This paper presents the first data on the Sr isotopic composition of groundwaters from the MCB. The results of this study have a bearing on questions related to the timing and origin of Pb–Zn and strontianite mineralizations within and in the periphery of the MCB, and are of direct interest to the small, but vibrant, salt-water spa industry in the area.

1.2. Geographic location

The MCB extends in N–S direction from 51°30′N to 52°20′N (ca. 150 km) and in W–E direction from 6°30′E to 9°E (ca. 80 km) and covers an area of close to 11,000 km^2 (Fig. 1). To the south, it is bordered by the mountain range of the Rhenish Schiefergebirge. To the east and northeast, the ridges of the Egge Mountains and the Osning form a sharp morphologic boundary. In the west, northwest and north, the transitions to the neighboring Lower Rhine area and the Central-Netherlands-Basin occur without a clear morphologic change.

Morphologically, the area of the MCB can be subdivided into lowlands, wide valleys, ridges, and mountains (Struckmeyer, 1990). The landsurface generally slopes from SE to N and NW. Elevation gradients mainly range between 0.1 and 1 %, and rarely exceed 2%. The highest elevations occur in the SE corner of the MCB (up to 503 m a.s.l.). At the western and northwestern margins of the basin,

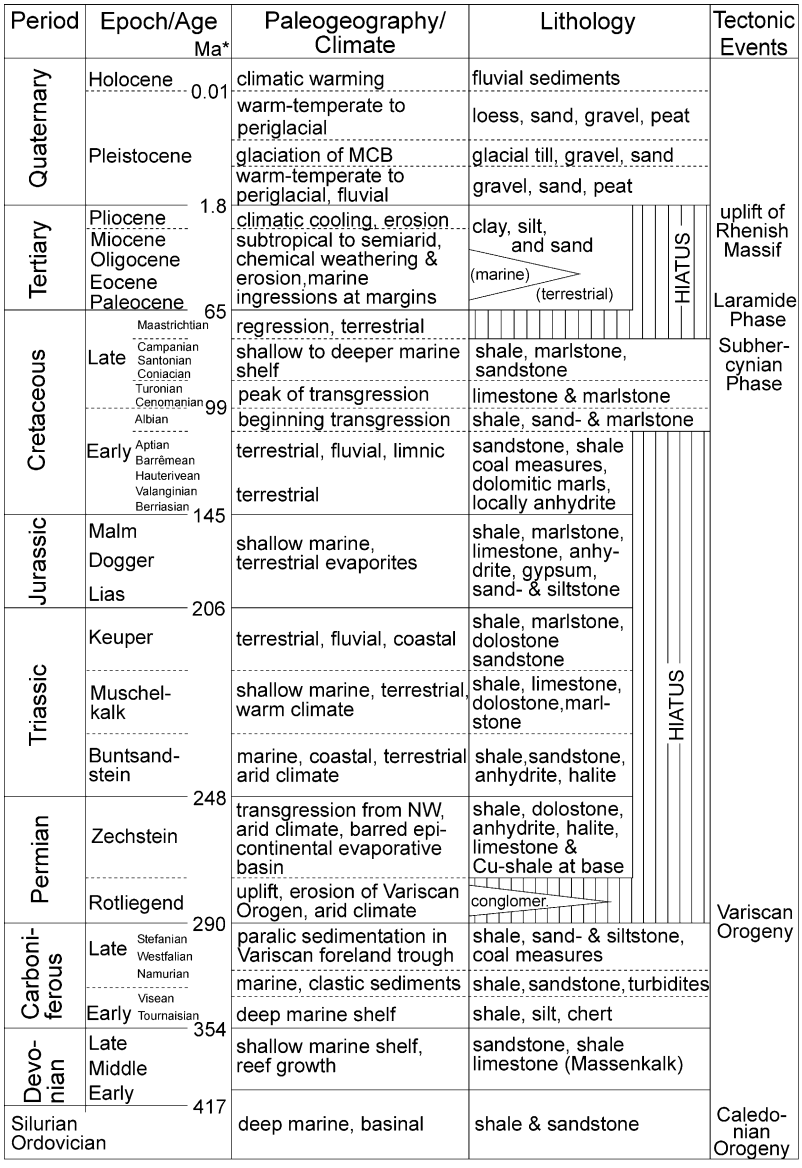

Fig. 2. Overview of the geologic history of the MCB (modified from Geologisches Landesamt Nordrhein-Westfalen (1995)). * Ages after Gradstein and Ogg (1996).

maximum elevations reach about 50 m a.s.l. Several areas within the MCB have elevations of up to 150 m a.s.l. and exhibit a strong local relief with deeply incised valleys. The remaining area of the MCB consists of extensive lowlands with elevations between 20 and 75 m a.s.l.

1.3. Geologic framework

An overview of the geologic history of the area of the MCB is shown in Fig. 2. In the subsurface, the MCB consists of two major geologic units: the Paleozoic basement and the overlying Mesozoic and Cenozoic strata (Fig. 3). The Paleozoic basement, which is generally referred to as the Rhenish Massif, consists of Ordovician to Upper Carboniferous, mainly clastic sedimentary rocks that were deformed during the Late Carboniferous Variscan Orogeny, resulting in SW–NE trending folds and thrust faults. The Variscan deformation front approached from the south, hence the intensity of deformation decreases northward. In the south, strongly deformed rocks of the Rhenish Massif crop out in the Rhenish Schiefergebirge. Paleozoic rocks that were not deformed during the Variscan Orogeny occur in the subsurface of the northwestern part of the MCB.

The central part of the Rhenish Massif was exposed at the surface during most of the post-Variscan time. Upper Permian to Lower Cretaceous sedimentary rocks, including Upper Permian (Zechstein), Lower Triassic (Röt), and Upper Triassic (Malm) halite deposits, occur only in the periphery of the MCB (Figs. 1 and 3). An Albian/Cenomanian

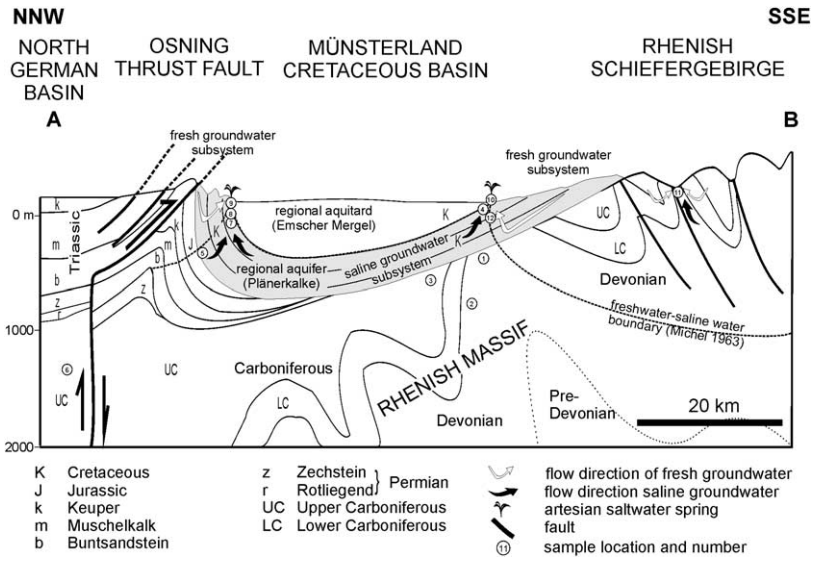

Fig. 3. Schematic cross-section A–B (see Fig. 1) depicting the stratigraphy and present-day geological structure of the MCB, as well as the position of the boundary between fresh and saline groundwater (TDS = 1000 mg/l) in the subsurface (dashed line). See text for further explanation.

transgression resulted in the inundation of the northern Rhenish Massif and marine sedimentation resumed. During the Cenomanian and Turonian, marine limestones, the so-called 'Plänerkalke' formed, followed by marls ('Emscher Mergel') of Coniacian to Campanian age. The MCB fell dry at the end of the Late Cretaceous, due to uplift and northward tilting of the Rhenish Massif. During the Tertiary, marine sedimentation took place only in the Lower Rhine area in the western part of the basin (Fig. 1).

Wrench tectonics during the Subhercynian and Laramide phases of the Saxonian Orogeny in the Late Cretaceous to Early Tertiary resulted in the present-day asymmetric structure of the basin, which is characterized by steeply dipping to overturned beds of the Plänerkalke at the northeastern and northern margins of the basin and gently sloping beds at its western, southern, and eastern margins (Fig. 3). During the Laramide phase of the Saxonian Orogeny, southward thrusting and transpressional uplift of fault blocks (e.g. Ibbenbüren fault block; Fig. 1, sample location 6) occurred along the so-called Osning Zone, which separates the MCB from the North German Basin to the north (Rosenfeld, 1983) (Fig. 3).

In the Pleistocene, the Scandinavian continental glaciers extended southward into the MCB in three phases during the Saale glacial period, crossing the mountain ridges of the Osning Zone (Thome, 1983). Glacial erosion and deposition resulted in characteristic glacial and periglacial sediments and landforms (glacial till, erratics, drumlins, kames, osers, sanders, loess plains), which are still present at the surface today.

1.4. Hydrogeologic framework

The regional hydrologic system of the MCB is that of an artesian basin that has elevated recharge areas at its margins and a thick and areally extensive aquitard overlying the regional aquifer in its center (Figs. 1 and 3). The main regional aquifer in the MCB consists of Upper Cretaceous (Cenomanian/Turonian) marine carbonates (Plänerkalke) (Fig. 3). Saline groundwaters also permeate the fractured bedrock of the underlying deformed Paleozoic basement, the so-called northern Rhenish Massif. In the center of the MCB, the Plänerkalke are overlain by Upper Cretaceous marls ('Emscher Mergel'), which form the regional aquitard that separates the regional aquifer from several local hydrologic systems close to the surface (Struckmeyer, 1990). Within the regional aquifer, two hydrologic subsystems have been recognized (Struckmeyer, 1990) (1) a marginal fresh groundwater subsystem at the southern, eastern, and northern margins of the basin where the regional aquitard has been eroded; and (2) a central saline groundwater subsystem below the regional aquitard (Fig. 3).

The sedimentary rocks of the Paleozoic basement generally have low hydraulic conductivities (k_f) that range from 2×10^{-13} to 4×10^{-9} m/s (Wedewardt, 1995) and are similar to those of the Upper Cretaceous regional aquitard ($k_f = 10^{-12}$–10^{-9} m/s; Struckmeier, 1990). Most of the groundwater movement in the Paleozoic basement and regional carbonate aquifer is restricted to fractures and faults (Wedewardt, 1995). In the marginal areas of the MCB, the karstification of the Upper Cretaceous limestones has enhanced permeabilities in the areas where the regional carbonate aquifer is not covered by the regional aquitard (Figs. 1 and 3). The fact that the saline groundwaters in the central part of the regional aquifer have not yet been diluted to fresh water salinities has been attributed to decreasing permeabilities within the regional aquifer from the margins to the center and to the effective sealing qualities of the regional aquitard (Struckmeyer, 1990).

The flow patterns within the regional saline groundwater subsystem are unknown because of the lack of pressure and hydrochemical data from the central part of the MCB (Struckmeyer, 1990; Wedewardt, 1995). In the few wells that penetrate the regional aquifer and the Paleozoic basement in the central part of the basin, no drill stem tests were carried out (Struckmeyer, 1990). Therefore, the possibility of lateral and vertical, cross-formational recharge of saline groundwaters from the underlying Paleozoic basement and neighboring areas along faults cannot be evaluated using hydrogeologic data.

The saline groundwaters discharge at the surface in artesian springs at the interface between the regional aquifer and the regional aquitard. They are also produced from wells from the regional aquifer and the underlying Paleozoic rocks below the aquitard. For example, in the deep coal mines of the Ruhr District in the southwestern part of the MCB, the saline groundwaters are being pumped continuously to allow mining activities to proceed and to keep abandoned sections of the mines accessible for possible reactivation (Wedewardt, 1995). In response to the extraction of saline groundwaters in coal mines during the last 150 years, the boundary between the fresh groundwater subsystem at the margins of the basin and the central saline groundwater subsystem has shifted basinward, resulting in the disappearance of saltwater springs at the surface (Struckmeyer, 1990).

Presently, the pressure exerted by meteoric water recharge of the regional fresh groundwater subsystem from the highlands in the Osning fault zone, Egge Mountains, and Rhenish Schiefergebirge (Figs. 1 and 3) on the regional saline groundwater subsystem appears to be the driving force for the artesian discharge of the saline groundwaters. After heavy rainfalls, the rate of discharge as well as the salinity of the discharging saline groundwater has been reported to increase (Angerer et al., 1968; Fricke, 1961, 1963, 1964b; Papakonstantinou, 1970), which indicates that more concentrated, saline waters are mobilized from greater depth.

Points of discharge at the surface and in the subsurface are almost exclusively reported to be associated with fault-related fracture systems (Fricke, 1961, 1963, 1964a,b, 1967, 1968; Michel, 1963; Wedewardt, 1995; Wolansky, 1964). Many of these faults cut through the Paleozoic basement and overlying Cretaceous bedrock and extend southward into the Rhenish Schiefergebirge. Although the boundary between fresh and saline groundwater (TDS $>$ 1000 mg/l) lies at greater depths in the Rhenish Schiefergebirge than in the MCB (Michel, 1963; Fig. 3), saline groundwaters ascend along fault planes and discharge at the surface, especially where NNW–SSE trending normal faults cross-cut the SW–NE trending anticlines (e.g. sample location 11 in Fig. 3; Fricke, 1967; Michel, 1983b).

Locally, the faults along which saline groundwaters occur are mineralized with base metal sulfides associated with quartz, barite, and carbonate gangue minerals (calcite, dolomite, strontianite) (Bode, 1980; Hofmann, 1979; Hofmann & Schürenberg, 1979; Pilger, 1961; Schaeffer, 1983, 1984; Scherp & Strübel, 1974; Unland, 1985). The Pb–Zn veins in the Paleozoic rocks of the Ruhr District have been thought to have resulted from the ascent of metal-bearing, hydrothermal fluids along faults during the late phases of the Variscan Orogeny under the influence of magmatic intrusions in the deeper subsurface (Pilger, 1961). More recent investigations of the tectonic evolution of the Ruhr District, however, indicate that many of these faults are of post-Variscan origin and that the major amount of the base metal sulfide mineralization may be of Cretaceous and Tertiary ages (Drozdzewski & Wrede, 1994).

2. Methods

For this study, 12 water samples were taken from locations at the margins of the MCB where saline groundwaters were accessible (Fig. 1, Table 1). Sample locations include subsurface coal mines in the Carboniferous of the Ruhr District (sample 3) and the Ibbenbüren District (sample 6), nine wells (six of those artesian), and one natural artesian spring (sample 10). The samples originate from a variety of depths (0 m to approximately 1500 m below surface), stratigraphic levels (Middle Devonian to Pleistocene), and aquifer lithologies (fractured shale, sandstone, limestone, sand) (Fig. 3; Table 1).

Prior to sampling, the temperature, pH, and specific electrical conductivity of the waters were measured electrometrically using downhole probes. The measured values have not been corrected for differences in temperature and, hence, can be used only as an approximation for the total concentration of dissociated ions.

The water samples were collected in airtight polyethylene bottles and special care was taken not to leave any headspace. Volumes taken were 500 ml for analysis of the hydrochemical composition and TDS, and 60 ml for isotopic analysis ($^{87}Sr/^{86}Sr$, $\delta^{18}O$, δD).

The results of previous hydrochemical analyses carried out by the Fresenius Institute were available for sample locations 1, 2, 4, and 9. Michel and Nielsen (1977) published sulfur isotope data for saline groundwaters at sample locations 1, 2, 4, 8, and 10. The sulfur isotope composition for a saline groundwater at sample location 5 was determined by Bässler (1970).

2.1. Hydrochemistry

The hydrochemical composition and TDS of the water samples were determined by Dr B. Lüer in the laboratory of the Geological Survey of the Province of Northrhine-Westfalia. Chloride and nitrate concentrations were determined by ion chromatography (IC), using a Dionex 4000i ion chromatograph and bicarbonate concentrations by titration with 0.1N HCl. Fluoride concentrations were measured electrochemically with an ion-selective electrode (ISE).

Table 1
Results of field measurements, analyses of chemical and isotopic composition of saline groundwater samples from the MCB

Sample number	1	2	3	4	5	6	7	8	9	10	11	12
Well/spring/mine	B 14N	Bad Waldliesborn I	Iduna-Quelle	Bad Westernkotten 1 (W. Warte)	Saline Gottesgabe	Ibbenbüren Ostfeld	Weidtmann-Sprudel	Neue Martins-Quelle	Wünschelbrunnen (Solbad Ravensberg)	Sültsoid 3	Kaiser-Heinrich-Quelle	Padulus (Schloss Neuhaus)
Location	Bad Sassendorf	Lippstadt	Bottrop-Kirchhellen	Erwitte	Rheine	Ibbenbüren	Bad Rothenfelde	Bad Laer	Borgholzhausen	Salzkotten	Warstein-Belecke	Paderborn
R	3441523	3454202	2560980	3455485	2596868	3417200	3442720	3437845	3448035	3472965	3453595	3480360
H	5718019	5731270	5718860	5722535	5796972	4796350	5775180	5775005	5773728	5725395	5706495	5734710
Depth (m)	411	910	658.5	79	440	1360 to 1560	83	160	13	0	33	192
Aquifer lithology	Shale/sandstone	Shale	Sandstone	Limestone	Shale	Limestone/ sandstone	Limestone	Limestone	Sand	Sand	Shale/sandstone	Limestone
Stratigraphy	Middle Devonian	Middle Devonian	Upper Carboniferous	Upper Cretaceous	Lower Cretaceous	Upper Carboniferous	Upper Cretaceous	Upper Cretaceous	Pleistocene	Pleistocene	Upper Devonian	Upper Cretaceous
Temperature (°C)	21.3	31.4	n.a.	n/a	n/a	n/a	16.6	??17.6	16.5	13.4	13.4	19.5
pH	6.6	6.3	n.a.	6.4	7.2	n/a	6.6	6.6	6.8	6.6	7.3	6.8
Conductivity (mS/m)	6690	9630	n.a.	n/a	1384	n/a	5390	6300	1973	2350	701	720
Na (mg/l)	29250	37420	13450	24600	14890	38660	17940	23000	5355	6366	1735	1425
K (mg/l)	506	650	121.76	482	86.887	185	248	306	84.971	104.42	51.471	23.75
Ca (mg/l)	1515	1811	2100	1636	395	1020	1435	1643	483	455	175.26	341
Mg (mg/l)	310	251	521	215	150	408	223	260	61.811	38.565	33.886	19.067
Fe (mg/l)	15.3	16.1	7.5	17	< 0.002	< 0.002	21.2	16.6	< 0.002	0.42	0.71	0.44
Mn (mg/l)	0.3	0.7	0.38	0.6	0.05	< 0.001	0.52	0.7	0.001	0.35	0.15	0.2
Cl (mg/l)	48000	60000	24500	40000	23500	62000	28000	36000	7900	9700	2800	2423
SO_4 (mg/l)	747	1370	1870	1263	< 0.199	939	2400	2997	843	462	95	136.67
HCO_3 (mg/l)	1183.7	1427.7	146.44	1598.6	573.56	445.42	2074.5	2257.5	1342.3	1183.7	378.3	567.45
NO_3 (mg/l)	< 0.499	< 0.499	< 0.499	< 0.499	< 0.499	< 0.499	< 0.499	< 0.499	< 0.499	< 0.499	< 0.499	7.269
Zn (mg/l)	0.005	0.104	0.013	0.009	0.005	3.6	0.012	0.017	0.034	0.002	0.006	0.144
Cu (mg/l)	< 0.003	0.25	< 0.003	< 0.03	< 0.003	< 0.003	< .003	< 0.003	< 0.003	< 0.003	< 0.003	0.008
Ni (mg/l)	0.012	0.1	0.02	0.037	0.007	0.02	0.026	0.03	0.013	0.021	0.004	0.009
Co (mg/l)	< 0.002	0.002	< 0.002	< 0.002	< 0.002	< 0.002	< 0.002	< 0.002	< 0.002	< 0.002	< 0.002	< 0.002
Sr (mg/l)	110	76.5	70	68.5	63.8	59.2	47.7	37	27.3	9.306	6.324	6.263
B (mg/l)	3.08	4.1	6.4	2.4	3.5	1.25	2.5	2.7	1.024	0.635	0.347	0.123
Cd (mg/l)	< 0.001	< 0.001	< 0.001	< 0.001	< 0.001	< 0.001	< 0.001	< 0.001	< 0.001	< 0.001	< 0.001	< 0.001
Cr (mg/l)	< 0.004	< 0.004	< 0.004	< 0.004	< 0.004	< 0.004	< 0.004	< 0.004	< 0.004	< 0.004	< 0.004	0.019
Pb (mg/l)	< 0.006	< 0.006	< 0.006	< 0.006	< 0.006	< 0.006	< 0.006	< 0.006	< 0.006	< 0.006	< 0.006	< 0.006
As (mg/l)	< 0.02	< 0.02	< 0.02	< 0.02	< 0.02	< 0.02	< 0.02	< 0.02	< 0.02	< 0.02	< 0.020	0.025
Ba (mg/l)	0.027	0.2	0.029	0.03	9.709	0.38	0.02	0.017	0.026	0.02	0.069	0.071
F (mg/l)	0.08	0.37	0.87	0.1	0.39	0.29	0.13	0.16	1.3	0.41	0.54	0.23
P (mg/l)	< 0.099	< 0.099	1.69	< 0.099	< 0.099	< 0.099	< 0.099	< 0.099	< 0.099	< 0.099	< 0.099	< 0.099
N (mg/l)	29.8	39.1	12.7	20	19.4	22.3	11.9	13.5	3.12	3.3	0.85	< 0.5
Al (mg/l)	0.015	< 0.005	0.114	0.124	0.021	0.064	0.07	0.117	0.038	0.016	0.019	0.025
Li (mg/l)	21.4	19.6	3.6	9.94	3.6	8.75	3.5	4.2	1.1	2.594	1.268	0.652
TDS (mg/l)	90764	112674	49600	83434	46586	116820	58208	72508	15694	18166	5726	5402
$^{87}Sr/^{86}Sr$	0.71165	0.71262	0.70845	0.71134	0.70883	0.71319	0.70945	0.71003	0.70883	0.71176	0.71357	0.71059
$\delta^{18}O$ (SMOW)	−7.8	−8.29	−4.56	−8.37	−6.28	−6.99	−8.8	−9.46	−8.92	−8.07	−8.63	-8.15
δD (SMOW)	−57.55	−59.28	−29.48	−55.01	−42.2	−45.32	−61.12	−62.1	−59.3	−55.72	−56.37	−52.79
$\delta^{34}S$ (CDT)[a]	13.5	14.5	–	13.3	11.2[b]	–	–	11.4[a]	–	10.8[a]	–	–
Comments	Well	Well, artesian	Zeche Prosper, near Krudenberg-Sprung	Well, artesian	Well	Subsurface coal mine	Well	Well	Well, artesian	Spring, artesian	Well, artesian	Well, artesian

[a] From Michel and Nielsen (1977).
[b] From Bässler (1970).

Bromine and iodine were not analyzed. Total sulfur and phosphorus concentrations and all cation concentrations were determined by inductively coupled plasma (ICP)-spectroscopy, using a Thermo Jarrel Ash (TJA) IRIS-AP ICP equipped with a charge injection device (CID)-detector in an argon plasma. The water samples were evaporated at 180 °C to determine the amount of TDS.

2.2. Stable isotope analysis

Determination of the oxygen and hydrogen isotopic composition of the water samples was carried out at the University of Calgary. The isotope composition of oxygen was determined by analysis of CO_2 that was equilibrated isotopically with the water at ambient temperature (at 25 °C). The isotope composition of hydrogen was measured by analysis of H_2 gas that was obtained by reacting the water samples with metallic zinc at 450 °C. The isotope compositions are reported in the δ-notation relative to the SMOW standard. In-run precision was better than $\pm 0.2‰$ for $\delta^{18}O$ and better than $\pm 1‰$ for δD.

2.3. Strontium isotope analysis

For each water sample, the volume of water required to yield 4 μg of strontium (necessary for accurate strontium isotopic analysis) was calculated based on the strontium concentrations of the water samples as determined by ICP. The necessary aliquot of water was evaporated and the residue dissolved in 1N HCl. Strontium was extracted from the solution using standard cation exchange techniques. The strontium isotopic analyses were carried out on a VG 354 thermal ionization mass spectrometer at the University of Alberta. The samples were loaded as a phospho-tantalate gel on a single Re ribbon bead assembly. In-run precision was better than 4×10^{-5} (2σ). The isotopic ratios of the samples were normalized against the value of the NBS 987 standard, which yielded a $^{87}Sr/^{86}Sr$ value of 0.71021 over the period of the analysis of the water samples.

3. Results

The results of the field measurements and of the chemical and isotopic analyses are tabulated in Table 1 and plotted in Figs. 4–11.

3.1. Temperature and pH

Temperature measurements could only be obtained for eight of the samples. The temperatures of the water samples range from 13.4 °C at the surface to 31.4 °C at 910 m depth (Fig. 4). The temperatures of six samples at shallow depths (between 0 and 192 m) are significantly elevated relative to those expected at their respective depths, based on the mean annual surface temperature of 8 °C and an assumed geothermal gradient of 3 °C/100 m (Fig. 4). The temperature of one sample at 411 m depth is only slightly elevated and that of one sample at 910 m depth is lower. The pH-values show a range from 6.3 to 7.3, irrespective of aquifer lithology (Table 1).

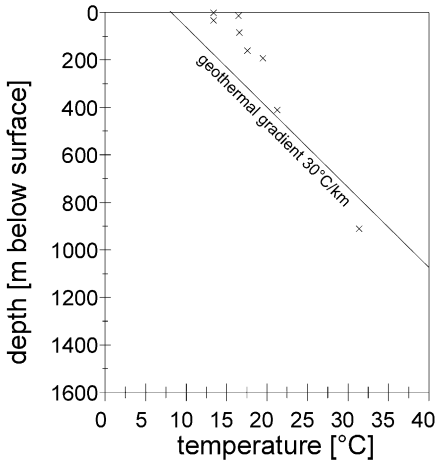

Fig. 4. Temperature vs. depth plot for the investigated saline groundwater samples from the MCB. The solid line represents the expected temperature increase with depth based on an average annual surface temperature of 8 °C and assuming a geothermal gradient of 30 °C per 1000 m.

3.2. Total dissolved solids and specific electrical conductivity

The TDS of the investigated water samples range from 5400 mg/l (sample 12) to 113,000 mg/l (sample 2), with eight out of 12 samples having higher TDS than seawater (approximately 35,000 mg/l; Drever, 1988). The specific electrical conductivity values correspond well with TDS. Generally, TDS increases with depth but the data scatter of the 12 samples is quite large (Fig. 5). Samples with higher TDS than seawater (group 1; samples 1 to 8) are from sample locations at greater depths where active mixing of meteoric water and saline groundwater is expected to be

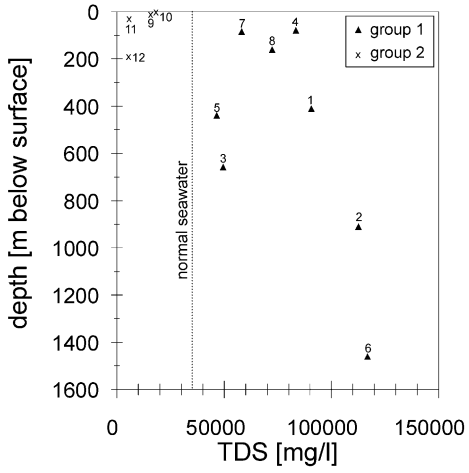

Fig. 5. Depth vs. TDS plot of the saline groundwater samples from the MCB. The samples have been divided into two groups: group 1 with TDS > normal seawater, and group 2 with TDS < normal seawater.

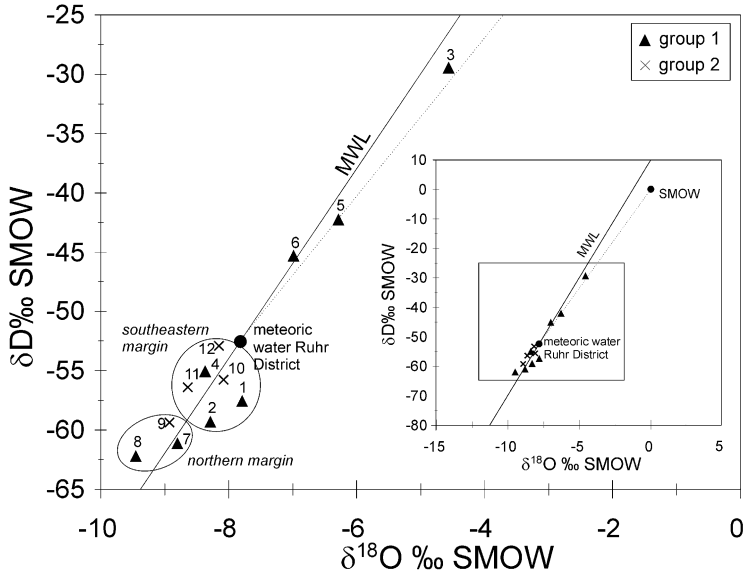

Fig. 6. Stable isotope compositions of saline groundwaters of the MCB. Samples from the northern and southeastern margins fall into distinct groups. See text for further explanation.

limited or non-existent. Samples with lower TDS than seawater are from sample locations at or close to the surface (group 2; samples 9 to 12) where active mixing can be expected.

3.3. Stable isotope composition

Oxygen and hydrogen isotopic analyses for the investigated saline groundwaters from the MCB are shown in Fig. 6 along with the global meteoric water line (MWL). Most of the samples plot on or very close to the MWL. The range of δD values for present-day shallow groundwaters of the area of the MCB is between −50 and −60‰ SMOW (Sonntag, Münnich, & Rozanski, 1983). Wedewardt (1995) reports a δD value of −52.5‰ SMOW and a $\delta^{18}O$ value of −7.82‰ SMOW for the present-day precipitation in the Ruhr District (Fig. 6). All samples of group 2 and the majority of samples of group 1 have δD values lower than that of present-day meteoric water in the Ruhr District, but fall within regional range. Samples from the northern margin of the MCB (samples 7–9; Figs. 1 and 3) have the lowest values, samples from the southeastern part have slightly higher values (samples 1, 2, 4, 10, 11, and 12). The data for sample 6 plot on the MWL, but at higher values than present-day precipitation. The data for samples 3 and 5 plot on a trajectory between the value for present-day meteoric water in the Ruhr District and that of seawater (SMOW). Of the samples of group 1, the two samples with the least elevated TDS have the highest δD and $\delta^{18}O$ values (samples 3 and 5).

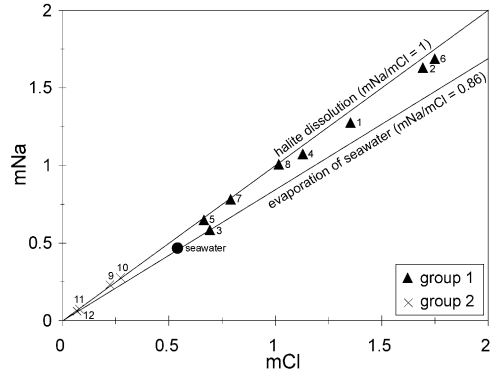

Fig. 7. Plot of molar concentrations of Na and Cl in the investigated samples.

3.4. Hydrochemical composition

The chemical composition of the analyzed water samples is characterized by the predominance of Na and Cl, which generally represent more than 90 equiv. mol% of the total cations and anions (Table 2). Seawater has a molar ratio of Na and Cl (*m*Na/*m*Cl) of about 0.86, whereas that of halite is 1. The *m*Na/*m*Cl ratios of the water samples range between 0.85 (sample 3) and 1.05 (sample 9), with most samples having ratios close to unity (Table 2; Fig. 7). Ca generally is the second most important cation and can reach up to 21.0 mol% of the total cations (sample 12) (Table 2). The two samples with the lowest *m*Na/*m*Cl ratios (samples 3 and 12) contain the largest molar quantities of Ca (14 and 21 mol% of total cations, respectively). Further anions that almost always occur as major constituents are SO_4 and HCO_3. Only sample 5 is devoid of measurable amounts of SO_4 (Fig. 8). In the same sample, Ba occurs as a major constituent (9.7 mg/l), whereas all other samples have Ba concentrations below 0.4 mg/l (Table 1). Concentrations of Fe and Li exceed 5 mg/l in 50 and 30% of the samples, respectively. The concentrations of all other ions vary

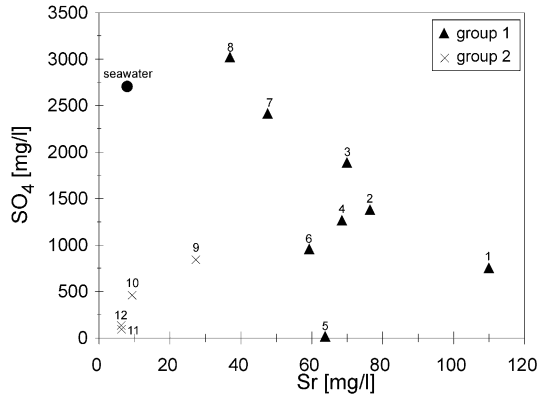

Fig. 8. Plot of SO_4 and Sr concentrations in the investigated samples.

from that of minor and that of trace constituents or are below their respective detection limit (Table 1).

With respect to seawater, all samples are depleted in Mg (Fig. 9a) and enriched in HCO_3 (not shown). Furthermore, the majority of samples is depleted in K (Fig. 9b) and SO_4 (Fig. 8) and enriched in Na, Ca, Sr, and Cl (Figs. 7, 8, 9c and d). Mg and K concentrations correlate positively with Cl concentrations (Fig. 9a and b). Sample 3 in the Mg/Cl plot and sample 3, 5, and 6 in the K/Cl plot do not fall on the main trends. In the Ca/Cl and Sr/Cl plots (Fig. 9c and d) the data scatter widely and only weak positive correlations are displayed. In the Ca/Cl plot, samples 3, 5, and 6 exhibit the largest deviations from the main trend. Since the chemical compositions of the waters are dominated by Na and Cl, very similar data distributions result when K, Mg, Ca, and Sr concentrations are plotted against Na concentrations (e.g. K/Na plot in Fig. 10a). The K/Na ratios of all samples are below that of seawater (K/Na = 0.037) (Table 2; Fig. 10b). Regardless of the Cl concentrations, the K/Na ratios of most samples fall within a range between 0.013 and 0.020. Exceptions to this are samples 3, 5, and 6 of group 1 with very low K/Na ratios, and sample 11 of group 2 with a high K/Na ratio (Fig. 10b). No systematic relationships between the chemical compositions and the stable isotope compositions of the investigated water samples could be identified.

3.5. Strontium isotope composition

The $^{87}Sr/^{86}Sr$ ratios of the investigated water samples range from 0.7084 to 0.7136. The values for samples from the regional aquifer (samples 4, 7, 8, 12) are above the range of values for Upper Cretaceous seawater (i.e. $^{87}Sr/^{86}Sr = 0.7073–0.7078$; Burke et al., 1982) and that for Phanerozoic seawater (i.e. $^{87}Sr/^{86}Sr = 0.7068–0.7090$; Burke et al., 1982), those from siliciclastic lithologies span a range from 0.7084 to 0.7136 (Table 1). With the

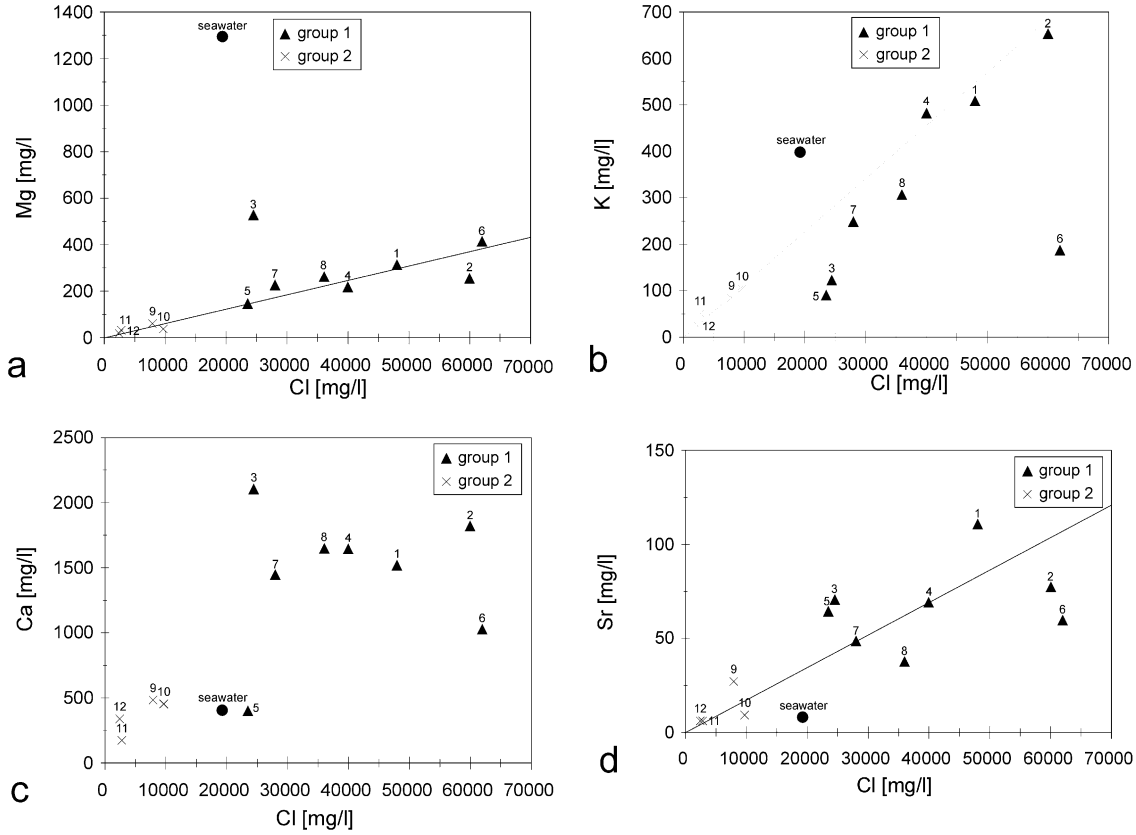

Fig. 9. Cross plots of Mg (a), K (b), Ca (c), and Sr (d) vs. Cl concentrations in the investigated samples.

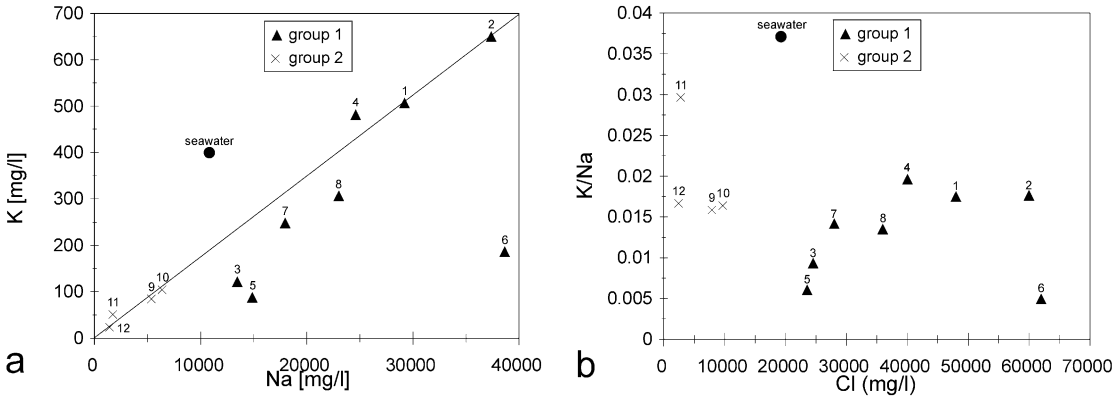

Fig. 10. Cross plots of (a) K and Na concentrations and (b) K/Na concentration ratios and Cl concentrations in the investigated samples.

exception of sample 3, water samples taken from the Paleozoic bedrocks have $^{87}Sr/^{86}Sr$ ratios higher than 0.7114, whereas samples taken from the overlying regional aquifer have $^{87}Sr/^{86}Sr$ ratios below 0.7114 (Fig. 11a). A water sample taken from Pleistocene sands above the steeply inclined regional aquifer at the northern margin of the MCB (sample 9; Figs. 1 and 3) has a $^{87}Sr/^{86}Sr$ ratio of 0.7088; another water sample from Pleistocene sands above the shallowly inclined regional aquifer in the southeastern part of the basin (sample 10; Figs. 1 and 2) has a $^{87}Sr/^{86}Sr$ ratio of 0.71176. Samples 7–9 from the northern margin form a trend of increasing $^{87}Sr/^{86}Sr$ ratios with increasing Cl concentration, which corresponds to an increase in depth.

For the samples of group 1, the $^{87}Sr/^{86}Sr$ ratios increase with increasing Cl concentrations (Fig. 11a). Since TDS is dominated by Na and Cl, TDS and Na concentrations exhibit the same positive correlation with the $^{87}Sr/^{86}Sr$ ratios

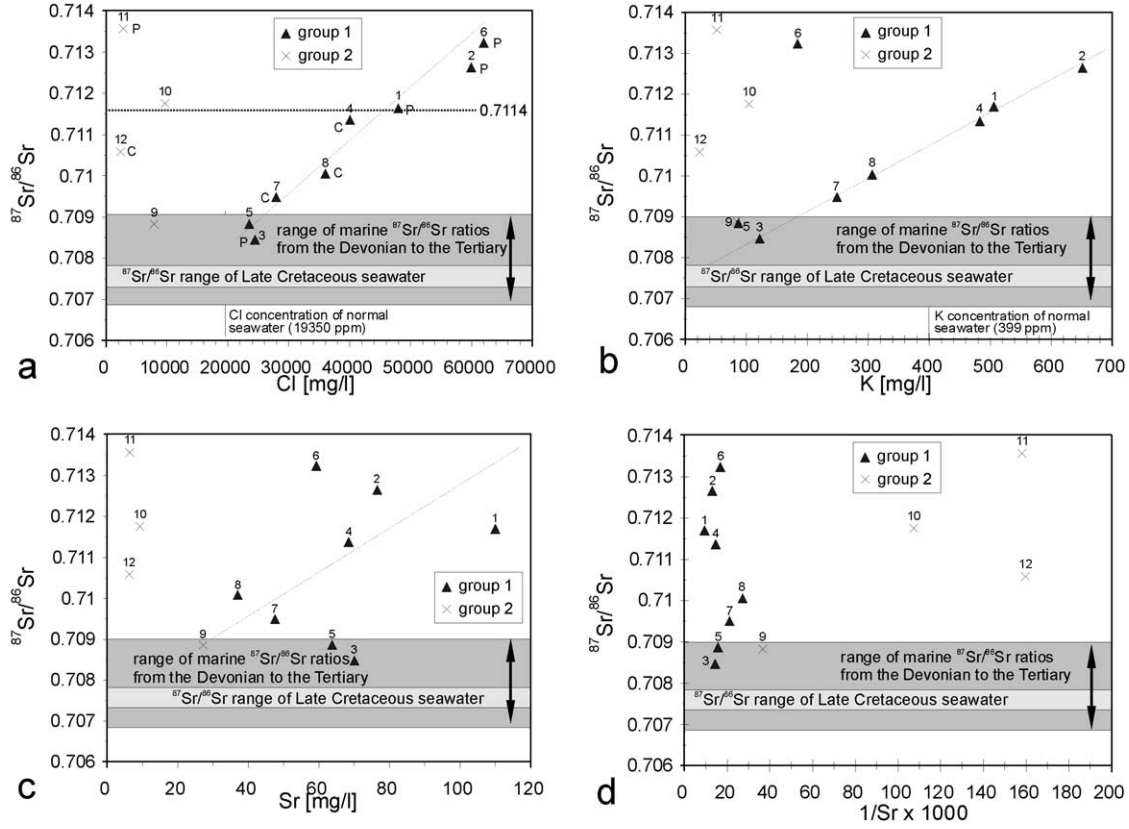

Fig. 11. $^{87}Sr/^{86}Sr$ ratio versus Cl (a), K (b), Sr (c), and reciprocal Sr (d) concentrations. With the exception of sample 3, water samples taken from the Paleozoic bedrocks (P) have $^{87}Sr/^{86}Sr$ ratios higher than 0.7114, whereas samples taken from the overlying regional aquifer (C) have $^{87}Sr/^{86}Sr$ ratios below 0.7114 (stippled horizontal line in (a). See text for further explanation.

Table 2
Molar percentages of major cations and anions, molar ratios of Na and Cl, and ratios of K and Na concentrations for samples from the MCB and seawater, calculated from values given in Table 1. Values for seawater were taken from Drever (1988)

Sample	Cations (equiv. mol%)				Anions (equiv. mol%)			*m*Na/*m*Cl	K/Na
	Na	K	Ca	Mg	Cl	SO_4	HCO_3		
1	91.8	0.93	5.45	1.84	97.5	1.12	1.40	0.94	0.017
2	92.7	0.95	5.15	1.18	97.0	1.64	1.34	0.96	0.017
3	79.5	0.42	14.24	5.83	94.4	5.32	0.33	0.85	0.009
4	90.5	1.04	6.91	1.50	95.6	2.23	2.22	0.95	0.020
5	95.0	0.33	2.89	1.81	98.6	0.00	1.40	0.98	0.006
6	95.0	0.27	2.87	1.90	98.5	1.10	0.41	0.96	0.005
7	89.0	0.72	8.17	2.09	90.4	5.72	3.89	0.99	0.014
8	90.0	0.70	7.38	1.92	91.1	5.60	3.32	0.99	0.013
9	88.1	0.82	9.12	1.92	84.9	6.69	8.39	1.05	0.016
10	90.7	0.87	7.43	1.04	90.4	3.18	6.41	1.01	0.016
11	85.5	1.49	9.90	3.16	90.6	2.27	7.12	0.96	0.030
12	76.4	0.75	20.96	1.93	84.9	3.54	11.56	0.91	0.017
Seawater	77.4	1.69	3.39	17.55	90.2	9.34	0.39	0.86	0.037

(not shown). With the exception of sample 6, these samples also form a trend of increasing $^{87}Sr/^{86}Sr$ ratios with increasing K concentrations (Fig. 11b). No correlation could be identified in the $^{87}Sr/^{86}Sr$ ratio versus Sr concentrations (Fig. 11c). In the plot of $^{87}Sr/^{86}Sr$ ratios vs. reciprocal Sr (1/Sr) concentration (Fig. 11d), the values for samples 10–12 of group 2 form a distinct group at high 1/Sr values and high $^{87}Sr/^{86}Sr$ ratios, whereas group 1 and sample 9 of group 2 scatter from low to high $^{87}Sr/^{86}Sr$ ratios at low 1/Sr values.

Of the samples of group 1, the two samples with the lowest $^{87}Sr/^{86}Sr$ (samples 3 and 5) have the highest δD and $\delta^{18}O$ values, which corresponds to the least elevated TDS (Fig. 5). For the samples of group 2, no obvious correlations between $^{87}Sr/^{86}Sr$ ratios, chemical and isotopic compositions could be determined. Sample 9, however, appears to fit into the trends described for the samples of group 1, because of its low $^{87}Sr/^{86}Sr$ ratio (Fig. 11b–d).

4. Discussion

The circumstance that the groundwater samples investigated in this study were taken from a variety of locations and lithologies implies that these samples are not necessarily representative of the saline groundwaters in the MCB. With this in mind, the principal aim of this discussion is to find a plausible explanation for the hydrochemical and isotopic characteristics that is consistent with the present knowledge of the geological and hydrogeological history of the area. Further investigations with a much larger database will have to be carried out to confirm the tentative interpretations presented herein.

4.1. Present-day movement of brines

The fact that the saline groundwaters at shallow depths have elevated temperatures relative to that expected at their respective depths (Fig. 4) and discharge on vertical faults (Fricke, 1961, 1963, 1964a,b, 1967, 1968; Michel, 1963; Wedewardt, 1995; Wolansky, 1964) serves as evidence for the upward movement of the saline groundwaters from deeper parts of the basin and the underlying Paleozoic bedrock on faults. Increases in salinity and rates of discharge of the saline groundwaters after heavy rainfalls (Angerer et al., 1968; Fricke, 1961, 1963, 1964b; Papakonstantinou, 1970) suggest that this upward movement is driven mainly by the pressure exerted by the regional fresh groundwater subsystem at the southern, eastern, and northern margins of the MCB on the regional saline groundwater subsystem in the centre of the basin (Figs. 1 and 3). The relative low temperature of the one sample at 910 m depth (sample 2), together with the fact that it originates from an artesian well and has a high salinity (TDS = 112,674 mg/l), suggests that it is not cooled (and diluted) by active mixing with surface-derived meteoric water, but rather that the geothermal gradient is probably lower than the assumed 30 °C/km (i.e. 26 °C/km).

4.2. Origin and evolution of the saline groundwaters

Based on the hydrochemical and isotopic data, the investigated saline groundwater samples fall into two groups. Samples in group 1 are characterized by TDS greater than seawater (Fig. 5), a wide range of stable isotope compositions between that of regional present-day meteoric water and seawater (Fig. 6), and increasing $^{87}Sr/^{86}Sr$ ratios with increasing Cl concentrations (Fig. 11a). Samples in group 2 have salinities less than seawater, stable isotope compositions in the range of present-day meteoric water in the region, and highly variable $^{87}Sr/^{86}Sr$ ratios.

4.2.1. Origin of the water

The fact that the oxygen and hydrogen isotope compositions of most of the investigated water samples plot on or close to the MWL (Fig. 6) indicates that these waters are dominated by present-day meteoric water. For samples of

group 2, this was to be expected, since they were obtained at locations where active mixing between present-day meteoric water and saline groundwaters is very likely (e.g. at the surface, at very shallow depths, and close to the boundary between fresh and saline groundwater). This is also reflected in their chemical compositions, especially their dilution below seawater salinities (Fig. 5). The fact that most of the samples of group 1 also have stable isotope compositions in the range of present-day meteoric water suggests that most of the regional aquifer and parts of the underlying Paleozoic units have been flushed by present-day meteoric water. Differences in the stable isotope compositions between samples from the southeastern margin (samples 1, 2, 4, 10–12) and those from the northern margin (samples 7–9) are probably due to regional and/or seasonal variations in the stable isotope composition of the precipitation in the respective recharge areas.

Mixing of water of a marine origin with meteoric water is suggested by the stable isotope compositions of samples 3 and 5, which plot on a trajectory connecting the stable isotope composition of present-day meteoric water in the Ruhr District with that of seawater (SMOW; Fig. 6). This is in agreement with the findings of Wedewardt (1995), who found a similar mixing trend in his investigation of the isotopic composition of the deep groundwaters in the Ruhr District. The fact that samples 3 and 5 are from the southwestern and northwestern margin of the MCB, which repeatedly experienced marine conditions during the history of the area (Fig. 2), supports this interpretation. Other processes, such as isotope exchange during water–rock interaction, evaporation and condensation, isotope fractionation due to membrane effects, and mixing of several different fluids, also can have an impact on the isotopic compositions of waters (Kharaka & Carothers, 1986). From the small data set available here, however, it is not possible to accurately evaluate the involvement of these processes.

The position of sample 6 on the MWL but at higher values than present-day meteoric water (Fig. 6) suggests the involvement of meteoric water from a time period when climatic conditions were warmer and/or when the area was located closer to the ocean (Faure, 1990; Sonntag et al., 1983). The Tertiary, for example, would satisfy both criteria (Fig. 2). Age determinations of some saline groundwaters from the MCB were carried out by Geyh and Michel (1981), Jacobshagen and Münnich (1964), and Wedewardt (1995). The absence of ^{14}C and ^{13}H in the samples with the highest salinities led Geyh and Michel (1981) and Jacobshagen and Münnich (1964) to the conclusion that the undiluted saline groundwaters are older than 40,000 years. In addition, Wedewardt (1995) reported the results of the isotopic analysis of the noble gases He and Ar from pore waters in Carboniferous sandstones and siltstones from the Ruhr District. Pre-glacial $^{40}Ar/^{36}Ar$-ratios (>300) and calculated semiquantitative He-ages between 24 and 45 Ma confirm a pre-glacial age of the saline groundwaters (Wedewardt, 1995).

These considerations suggest that three water components occur in the saline groundwaters of the MCB: (1) a seawater component; (2) an 'old' (pre-glacial) meteoric water component, and (3) a present-day meteoric water component. The present-day meteoric water component is dominant in most samples. In the deeper parts of the basin (sample 5) and the underlying Paleozoic (samples 3 and 6), however, undefined quantities of fluids that have the stable isotopic compositions of older meteoric water and seawater, respectively, appear to be present.

4.2.2. Dissolution of halite

Dissolved chloride can be used as the conservative reference parameter because in many halite-free environments few processes other than mixing affect its concentration (Hanor, 1987). High sodium and chloride concentrations in groundwaters generally suggest their origin from evaporated seawater or from the dissolution of evaporites. The slight enrichment of sodium with respect to evaporated seawater (Fig. 7) indicates an external source of sodium, provided there is no halite in the sequence that may have dissolved. Sodium is released into solution during weathering of Na-rich plagioclase (Wedepohl, 1978) and by cation exchange with Ca that is attached to the surfaces of newly formed clay minerals (Matthess, 1990). Alternatively, groundwaters that are enriched in Na with respect to evaporated seawater may also originate from the dissolution of halite. A brine that resulted from the dissolution of halite has a mNa/mCl ratio of about 1 (Lehmann, 1974; Zhou & Li, 1992). Halite dissolution is suggested by the fact that most of the investigated samples have ratios close to unity (Fig. 7). The fact that the samples with the lowest mNa/mCl ratios (samples 3 and 12) contain the largest molar quantities of Ca (14 and 21 mol% of total cations, respectively) (Table 2), suggests that, in these cases, dissolved Na was extracted from solution by exchange with Ca from clay minerals (Matthess, 1990).

Dissolution of halite as the main source for the sodium and chloride in the saline groundwaters in the MCB has been suggested by several authors (Fricke, 1961; Michel & Nielsen, 1977; Wedewardt, 1995). Supporting evidence has been provided by sulfur isotope measurements of the dissolved sulfate in saline groundwaters from the eastern and northeastern part of the MCB and adjacent areas (Bässler, 1970; Michel & Nielsen, 1977) (Table 1). Their data indicate that the sulfate in some of the saline groundwaters in the MCB originated from anhydrite in the Upper Permian (Zechstein) evaporites. The $\delta^{34}S$ value for Upper Permian sulfate is well constrained at about $+11 \pm 2‰$ CDT, and represents the minimum for marine sulfate during the Phanerozoic (Claypool, Holser, Kaplan, Sakai, & Zak, 1980; Kampschulte, Buhl, & Strauss, 1998). The $\delta^{34}S$ values of dissolved sulfate from saline groundwaters at the sample locations 1, 2, 4, 5, 8, and 10 range between 10.8 and 14.5‰ CDT (Table 1). The samples with $\delta^{34}S$ values between 8 and 13‰ CDT were considered to have obtained

their dissolved sulfate from the dissolution of Upper Permian evaporites (samples 5, 8, and 10), those with slightly higher values were considered to have been influenced by influx of dissolved Upper Permian marine sulfate (samples 1, 2, and 4) (Michel & Nielsen, 1977). Higher values may be due to mixing of Upper Permian marine sulfate with older or younger marine sulfate with higher $\delta^{34}S$ values and/or sulfate that had been affected by bacterial sulfate reduction (producing sulfide with low $\delta^{34}S$ values and leaving sulfate with higher $\delta^{34}S$ values).

Wedewardt (1995) used Br/Cl ratios of saline groundwaters from the Ruhr District as the main argument for the hypothesis that they derive their salinity from the subrosive dissolution of halite. Normal seawater has a Br concentration of about 67 mg/l and a Br/Cl ratio of about 0.0034. This ratio remains the same during evaporation of seawater up to halite saturation. When halite saturation is reached, Cl preferentially precipitates as NaCl, and Br preferentially remains in solution, resulting in Br/Cl ratios below that of seawater in the solid halite, and a continuous increase in the Br/Cl ratio in the remaining solution during further precipitation of chlorides. Depending on the Br concentration in the solution from which halite precipitated, the Br/Cl ratios in solid halite range between 0.0001 and 0.0004 (Rittenhouse, 1967). Consequently, the Br/Cl ratio of a brine that results from the dissolution of halite is smaller than 0.0034.

Wedewardt (1995) reported Br/Cl ratios between 0.0007 and 0.0029 (average 0.0014) for the saline groundwaters in the Ruhr District. From the chemical data of saline groundwaters in the Ibbenbüren District presented in Bässler (1970), Wedewardt (1995) calculated Br/Cl ratios ranging from 0.0003 to 0.0014. Previous chemical analyses of groundwater samples from sample locations 1, 2, 4, and 9 by the Fresenius Institute give Br/Cl ratios between 0.0004 and 0.0005.

It is, therefore, most likely, that the elevated *m*Na/*m*Cl ratios of the majority of samples from this study are the result of the subrosion of halite in the periphery of the MCB. In addition, there are local variations due to clay mineral exchange reactions, such as the low *m*Na/*m*Cl ratios of sample 3 and 12 (Table 2; Fig. 7).

4.2.3. Sources of Sr

The main sources of Sr are carbonate minerals, calcium sulfates (gypsum, anhydrite), plagioclase, and smectite, which have relatively high Sr concentrations but generally low $^{87}Sr/^{86}Sr$ ratios similar to that of the fluid (i.e. water or magma) from which they formed. Illite, K-feldspar, and mica contribute less Sr because they are more resistant to chemical weathering have low Sr concentrations, or both. These minerals, however, contain significant amounts of ^{87}Rb and, thus, produce radiogenic ^{87}Sr, resulting in $^{87}Sr/^{86}Sr$ ratios that increase with age. In a context where evaporites are present, the mineral sylvite (KCl), which contains only small amounts of Sr but has been reported to reach $^{87}Sr/^{86}Sr$ ratios up to 2.5 (Baadsgaard, 1987) as a result of high original ^{87}Rb concentrations, needs to be considered as a source of radiogenic Sr as well (Moldovanyi, Walter, & Land, 1993). All of the above minerals are present in the sedimentary succession of the area of the MCB and may have contributed Sr to the saline groundwaters.

In the area of the MCB, marine carbonates are the most likely source for Sr with marine $^{87}Sr/^{86}Sr$ ratios, because of their widespread occurrence and high Sr concentrations. For example, Kramm (1985) reported extremely uniform Sr isotopic compositions ($^{87}Sr/^{86}Sr = 0.70752 \pm 5 \times 10^{-5}$) from vein strontianite from carbonate-hosted deposits in the MCB. The fact that this $^{87}Sr/^{86}Sr$ ratio of the strontianite corresponds to that of the Upper Cretaceous (Campanian) host limestones within analytical error led Kramm (1985) to conclude that the Sr was derived from these limestones.

Calcium sulfates (gypsum, anhydrite) which are present in the periphery of the MCB (Fig. 2), may have contributed Sr with marine $^{87}Sr/^{86}Sr$ ratios as well. This is supported by the sulfur isotopic compositions of dissolved sulfate in saline groundwaters from the MCB, which have been interpreted to be derived from the dissolution of Zechstein evaporites (Michel & Nielsen, 1977).

The positive correlation between the $^{87}Sr/^{86}Sr$ ratios and K concentrations for the samples in group 1 (Fig. 11b) confirms that radiogenic Sr is derived from K-bearing minerals, but does not aid in distinguishing between the various possible sources. Clastic sedimentary rocks in the MCB make up most of the Paleozoic basement and are abundant in the Mesozoic sedimentary successions (Fig. 2) and are therefore the most likely source for the radiogenic Sr in the saline waters in the MCB. Sylvite only occurs along the periphery of the basin and, despite its potentially high $^{87}Sr/^{86}Sr$ ratios (Baadsgard, 1987), is probably volumetrically negligible. Furthermore, dissolution of sylvite causes enrichment of the groundwater in K relative to Na, which results in a positive correlation between the K/Na ratio and Cl concentration. For the investigated samples, such a correlation does not exist (Fig. 10b). The fact that most of the water samples obtained from the Paleozoic basement have $^{87}Sr/^{86}Sr$ ratios above 0.7114 while those from the overlying Cretaceous strata have lower ratios (Fig. 11a) suggests that the radiogenic Sr probably is derived mainly from interaction of groundwater with Paleozoic siliciclastic sediments.

4.2.4. Mixing relations and effects of water–rock interactions

The trend of increasing $^{87}Sr/^{86}Sr$ ratios with increasing Cl concentrations in group 1 (Fig. 11a) suggests mixing of a highly saline, ^{87}Sr-enriched water component and a less saline water component with a Sr isotope composition in the range of Phanerozoic seawater. Two-component mixing and endmember water compositions can be evaluated using plots of $^{87}Sr/^{86}Sr$ ratio vs. Sr concentration (Fig. 11c) and

$^{87}Sr/^{86}Sr$ vs. reciprocal Sr (1/Sr) concentration (Fig. 11d) (Faure, 1990). Mixing between two endmember fluids with different Sr concentrations and different $^{87}Sr/^{86}Sr$ ratios result in a hyperbolic mixing line in the $^{87}Sr/^{86}Sr$ ratio vs. Sr concentration plot, and in a straight line in the $^{87}Sr/^{86}Sr$ ratio vs. reciprocal Sr (1/Sr) concentration plot (Faure, 1990).

The scatter of data in the $^{87}Sr/^{86}Sr$ ratio vs. Sr concentration plot (Fig. 11c) suggests that processes other than simple mixing of Sr derived from two sources with different Sr concentrations and different $^{87}Sr/^{86}Sr$ ratios (e.g. carbonates and siliciclastics) have taken place. This is further confirmed by the scatter of data in the plot of $^{87}Sr/^{86}Sr$ ratios vs. 1/Sr concentration (Fig. 11d). Local processes involving addition or removal of Sr after mixing may be responsible for the lack of correlation. This is indicated by the scatter of data in the SO_4 vs. Sr, Ca vs. Cl, and Sr vs. Cl plots (Figs. 8, 10a and b). Addition of Sr from interaction with carbonates, sulfates, and siliciclastics may change the $^{87}Sr/^{86}Sr$ ratio of the groundwater (depending on the amount and the $^{87}Sr/^{86}Sr$ ratio of the added Sr relative to those of the Sr already present), whereas removal of Sr by precipitation of carbonates and sulfates will not affect its $^{87}Sr/^{86}Sr$ ratio.

$^{87}Sr/^{86}Sr$ ratios of the groundwater samples from the Paleozoic bedrocks are generally high, those from the groundwater samples from the overlying regional aquifer are lower, but do not fall within the range of $^{87}Sr/^{86}Sr$ ratios for Phanerozoic seawater (Fig. 11 a–d). This suggests that the waters must have contained Sr with high $^{87}Sr/^{86}Sr$ ratios prior to entering the regional aquifer and since then have not interacted enough with the limestones as to lower the $^{87}Sr/^{86}Sr$ ratios to marine values, and can be taken as further evidence for the upward movement of warm, saline (and ^{87}Sr-enriched) groundwaters along faults from the Paleozoic bedrock into the regional aquifer. The absence of water–rock Sr isotopic equilibration has been frequently observed in carbonate-hosted groundwaters, such as oil field brines, and has been interpreted in a similar way (Chaudhuri, Broedel, & Clauer, 1987; Connolly, Walter, Baadsgard, & Longstaffe, 1990; Moldovanyi et al., 1993; Stueber, Pushkar, &, Hetherington, 1984). The difference in the $^{87}Sr/^{86}Sr$ ratios between samples 9 and 10 (e.g. Fig. 11a) may be due to the difference in the vertical distance from the base of the regional aquifer to the point of discharge between the northern and the southeastern part of the MCB (Fig. 2). At sample location 9, the groundwater ascended through about 800 m of Upper Cretaceous limestones, whereas at sample location 9, the groundwater passed through only a vertical distance of 300 m, resulting in a relatively low $^{87}Sr/^{86}Sr$ ratio for sample 9 and a relatively high $^{87}Sr/^{86}Sr$ ratio for sample 10 (Fig. 11a).

The low $^{87}Sr/^{86}Sr$ ratio of sample 3 is probably due to interaction of groundwater with Paleozoic and/or Mesozoic marine carbonates or sulfates and mixing with seawater prior to entering the Carboniferous sandstone aquifer, from which the sample was obtained. For this sample, mixing with seawater-derived groundwater (either as original, syn-sedimentary pore water, or as younger seawater that infiltrated the Paleozoic sedimentary rocks) is indicated by its stable isotope composition (Fig. 6).

In the $^{87}Sr/^{86}Sr$ ratios vs. 1/Sr concentration plot (Fig. 11d), the values for samples 10, 11, and 12 of group 2 form a distinct group at high 1/Sr values and high $^{87}Sr/^{86}Sr$ ratios, which suggests dilution by meteoric water or dilute shale water (Chaudhuri & Clauer, 1993; Connolly et al., 1990). While the samples of group 2 follow the same trend in the K vs. Na concentration plot like samples of group 1 (Fig. 10c), they do not in the $^{87}Sr/^{86}Sr$ ratio vs. K concentration plot (Fig. 11b). Assuming that the water samples in group 2 originated from waters of group 1, this indicates that these water samples were affected by a process that decreased both their Na and K concentrations, but did not significantly change their K/Na ratios and $^{87}Sr/^{86}Sr$ ratios, which can only be achieved by dilution with meteoric water.

5. Conclusions

The chemical and isotopic data presented here confirm that the present-day saline groundwaters in the MCB are the combined result of water–rock interaction, migration, and mixing of fluids of different origins. Within the context of the regional geologic and hydrogeologic knowledge, the data provide evidence for: (1) halite dissolution, (2) water–rock interaction of highly saline fluids with siliciclastic sediments, (3) mixing of highly saline fluids with less saline waters of marine isotopic compositions, and (4) mixing of highly saline fluids with less saline waters of marine isotopic compositions, (5) fault-controlled movement of warm saline ^{87}Sr-enriched groundwaters from the Paleozoic bedrock into the overlying Late Cretaceous limestone aquifer, (6) water–rock interaction of ascending saline groundwater with the limestone aquifer, and (7) dilution by meteoric water.

The subrecent processes of mixing of different saline groundwaters, water–rock interaction, and dilution by modern meteoric water are volumetrically predominant. Old meteoric water of presumed Tertiary age (sample 6) and marine-derived water of presumed Cretaceous age (samples 3 and 5) are still present in the deeper parts of the basin and the underlying basement. The findings of this study can be used to refine our understanding of the origin and evolution of the saline groundwaters in the MCB. However, further hydrogeological, chemical and isotopic data, particularly from the deeper parts of the basin and the underlying Paleozoic rocks, are needed to confirm and extend the interpretations presented here.

Acknowledgements

This study was financially supported by funds from a Natural Science and Engineering Research Council

(NSERC) operating grant to HGM, supplemented by a research grant from the American Association of Petroleum Geologists (AAPG) to MG. The authors are indebted to Dr Heinrich Heuser (Geologisches Landesamt Nordrhein-Westfalen, Krefeld, Germany) for logistic support during sampling. Comments and suggestions by Dr Yousif Kharaka and one anonymous reviewer were greatly appreciated and helped to improve the manuscript.

References

Angerer, P., Michel, G., & Semmler, W. (1968). Das Verschließen der Solquelle Nateln. *Glückauf (Forschungshefte)*, *29*, 43–50.

Baadsgaard, H. (1987). Rb–Sr and K–Ca isotope systematics in minerals from potassium horizons in the Prairie Evaporite Formation, Saskatchewan, Canada. *Chemical Geology*, *66*, 1–15.

Bässler, R. (1970). Hydrogeologische, chemische und Isotopen-Untersuchungen der Grubenwässer des Ibbenbürener Steinkohlenreviers. *Zeitschrift der Deutschen Geologischen Geselschaft, Sonderhefte Hydrogeologie Hydrogeochemie*, 209–286.

Bethke, C. M., & Marshak, S. (1990). Brine migration across North America—the plate tectonics of groundwater. *Annual Reviews in Earth and Planetary Sciences*, *18*, 287–316.

Bode, R. (1980). Strontianit aus dem Münsterland. *Mineralogical Magazine*, *4*, 88–90.

Burke, W. H., Denison, R. E., Hetherington, E. A., Koepnik, R. B., Nelson, H. F., & Otto, J. B. (1982). Variation of seawater $^{87}Sr/^{86}Sr$ throughout Phanerozoic time. *Geology*, *10*, 516–519.

Carpenter, A. B. (1978). Origin and chemical evolution of brines in sedimentary basins. *Oklahoma Geological Survey Circular*, *79*, 60–77.

Chaudhuri, S., & Clauer, N. (1993). Strontium isotopic compositions and potassium and rubidium contents of formation waters in sedimentary basins: Clues to the origin of the solutes. *Geochemica Cosmochimica Acta*, 57.

Chaudhuri, S., Broedel, V., & Clauer, N. (1987). Strontium isotopic evolution of oil field waters from carbonate reservoir rocks in Bindley field, central Kansas, USA. *Geochimica et Cosmochimica Acta*, *51*, 45–54.

Claypool, G. E., Holser, W. T., Kaplan, I. R., Sakai, H., & Zak, I. (1980). The age curves of sulfur and oxygen isotopes in marine sulfate and their mutual interpretation. *Chemical Geology*, *28*, 199–260.

Connolly, C. A., Walter, L. M., Baadsgard, H., & Longstaffe, F. J. (1990). Origin and evolution of formation waters, Alberta Basin, Western Canada Sedimentary Basin. II. Isotope systematics and water mixing. *Applied Geochemistry*, *5*, 397–413.

Drever, J. I., (1988). The geochemistry of natural waters, 2nd Edition. Englewood Cliffs, NS: Prentice Hall.

Drozdzewski, G., & Wrede, V. (1994). Faltung und Bruchtektonik—analyse der tektonik im subvariscikum. *Fortschritte in der Geologie von Rheinland und Westfalen*, *38*, 7–187.

Faure, G. (1990). *Principles of isotope geology*, New York: Wiley.

Freeze, R. A., & Cherry, J. A. (1979). *Groundwater*, Englewood Cliffs, NJ: Prentice Hall.

Fricke, K. (1961). Tiefenwasser, Solquellen und Solewanderung im Bereich des Münsterschen Beckens. *Zeitschrift der deutschen geologischen Gesellschaft*, *113*, 37–47.

Fricke, K. (1963). Die neuen Solebohrungen der Saline und Solbad Sassendorf GmbH., zugleich Beitrag zur Hydrogeologie der Solevorkommen am Südrand des Münsterschen Beckens. *Heilbad und Kurort*, *15*, 102–108.

Fricke, K. (1964a). Neue Bohrungen und hydrogeologische Untersuchungen im Heilquellengebiet von Solbad Ravensber/Teutoburger Wald. *Heilbad und Kurort*, *16*, 116–118.

Fricke, K. (1964b). Bemerkungen zu den Solquellen des Hellwegs. (Erläutert am Beispiel Bad Westernkotten, Krs. Lippstadt.). *Zeitschrift der deutschen geologischen Gesellschaft*, *116*, 76–87.

Fricke, K. (1967). Das Heilquellengebiet von Bad Belecke (Möhne) und die Neuerschließung von Natrium-Chlorid-Wasser 1963. *Geologisches Jahrbuch*, *84*, 735–754.

Fricke, K. (1968). Hydrogeologische und hydrochemische Ergebnisse der Sole-Neubohrung (1965) Bad Westernkotten. *Fortschritte der Geologie von Rheinland und Westfalen*, *16*, 121–132.

Fricke, K. (1969). Die Thermalbohrung Bad Lippspringe 1962 (Martinus-Quelle). *Fortschritte in der Geologie von Rheinland und Westfalen*, *17*, 95–130.

Fricke, K., & Wevelmeyer, W. (1960). Neue Thermal-Sole-Bohrung in Bad Waldliesborn 900 m tief. *Heilbad und Kurort*, *12*, 158–162.

Geologisches Landesamt Nordrhein-Westfalen (1995). *Geologie im Münsterland*, 195 pp.

Geyh, M., & Michel, G. (1974). Isotopen-und Hydrochemie des tieferen Grundwassers im Raum Paderborn. *Fortschritte in der Geologie von Rheinland und Westfalen*, *20*, 67–77.

Geyh, M., & Michel, G. (1981). Isotopen- und hydrochemischen Betrachtungen über die Süßwasser/Salzwasser-Zone am Nordostrand des Münsterländer Beckens. *Zeitschrift der deutschen geologischen Gesellschaft*, *132*, 597–612.

Gradstein, F. M., & Ogg, J. (1996). A Phanerozoic time scale. *Episodes*, 19.

Graf, D. L. (1982). Chemical osmosis, reverse chemical osmosis, and the origin of subsurface brines. *Geochimica et Cosmochimica Acta*, *46*, 1431–1448.

Hanor, J. S., (1987). Origin and migration of subsurface sedimentary brines. SEPM Short course No. 21, USA.

Hardie, L. A. (1990). The roles of rifting and hydrothermal $CaCl_2$ brines in the origin of potash evaporites: a hypothesis. *American Journal of Science*, *290*, 43–106.

Hofmann, R. (1979). Die Entwicklung der Abscheidungen in den gangförmiger Barytvorkommen in Deutschland. *Monograph Series Mineral Deposits*, *17*, 81–214.

Hofmann, R., & Schürenberg, H. (1979). Geochemische Untersuchungen gangförmiger Barytvorkommen in Deutschland. *Monograph Series Mineral Deposits*, *17*, 1–80.

Jacobshagen, V., & Münnich, K. O. (1964). ^{14}C-Altersbestimmung und andere Isotopen-Untersuchungen an Thermalsolen des Ruhrkarbons. *Neues Jahrbuch der Geologie und Paläontologie, Monatshefte*, 561–568.

Kampschulte, A., Buhl, D., & Strauss, H. (1998). The sulfur and strontium isotopic compositions of Permian evaporites from the Zechstein basin, northern Germany. *Geologische Rundschau*, 192–199.

Kesler, S. E., Vennemann, T. W., Frederickson, C., Breithaupt, A., Vazquez, R., & Furman, F. C. (1997). Hydrogen and oxygen isotope evidence for origin of MVT-forming brines, southern Appalachians. *Geochimica et Cosmochimica Acta*, *61*, 1513–1523.

Kharaka, Y. K., & Carothers, W. W. (1986). Oxygen and hydrogen isotope geochemistry of deep basin brines. In P. Fritz & J. Ch. Fontes, *Handbook of environmental isotope geochemistry*, *Vol. 2*, (pp. 305–360). New York: Elsevier.

Kramm, U. (1985). Sr-Isotopenuntersuchungen zur Genese der Strontianitlagerstätte Münsterland/Westfalen. *Fortschritte in der Mineralogie, Beihefte*, *63*, 1.

Land, L. S., & Prezbindowski, D. R. (1981). The origin and evolution of saline formation water, Lower Cretaceous carbonates, south-central Texas, USA. *Journal of Hydogeology*, *54*, 51–74.

Lehmann, H.-W. (1974). Geochemie und Genesis der Tiefenwässer der Norddeutschen Senke. *Zeitschrift der angewandten Geologie*, *20*, 502–509, see also pages 551–557.

Lowry, R. M., Faure, G., Mullet, D. I., & Jones, L. M. (1988). Interpretation of chemical and isotopic compositions of brines based on mixing and dilution, Clinton sandstones, eastern Ohio, USA. *Applied Geochemistry*, *3*, 177–184.

Matthess, G. (1990). *Die Beschaffenheit des Grundwassers*, *Lehrbuch der Hydrogeologie, Band 2*. Berlin: Springer.

Michel, G. (1963). Untersuchungen über die Tiefenlage der Grenze Süsswasser-Salzwasser im nördlichen Rheinland und anschliessenden Teilen Westfalens, zugleich ein Beitrag zur Hydrogeologie und Chemie des tiefen Grundwassers. *Forschungsberichte des Landes Nordrhein-Westfalen*, *1239*, 131.

Michel, G. (1983a). Sole im Münsterland—woher, wohin? *Heilbad und Kurort*, *35*, 66–76.

Michel, G. (1983b). Die Sole des Münsterländer Kreide-Beckens. *Neues Jahrbuch der Geologie und Paläontologie, Abhandlungen*, *166*, 139–159.

Michel, G. (1994). Wie kommt die Sole ins Revier. *Mitteilungen der Geologischen Gesellschaft Essen*, *12*, 65–81.

Michel, G., & Nielsen, H. (1977). Schwefel-Isotopenuntersuchungen an Sulfaten ostwestfälischer Mineralwässer. *Fortschritte der Geologie von Rheinland und Westfalen*, *26*, 185–227.

Michel, G., Rabitz, A., & Werner, H. (1974). Betrachtungen über die Tiefenwässer im Ruhrgebiet. *Fortschritte der Geologie von Rheinland und Westfalen*, *20*, 215–236 with a contribution by Scherp A.

Moldovanyi, E. P., Walter, L. M., & Land, L. S. (1993). Strontium, boron, oxygen, and hydrogen isotope geochemistry of brines from basal strata of the Gulf Coast sedimentary basin, USA. *Geochimica et Cosmochimica Acta*, *57*, 2083–2099.

Morrow, D. W. (1998). Regional subsurface dolomitization: Models and constraints. *Geoscience Canada*, *25*, 57–70.

Papakonstantinou, A. (1970). *Die hydrogeologischen Verhältnisse im Raum Bad Westernkotten, Haarstrang (unter besonderer Berücksichtigung quantitativer und qualitativer Zusammenhänge zwischen Niederschlägen und Soleführung)*. Unpublished Diplom-Thesis, University of Marburg, 66 pp.

Patteisky, K. (1954). Die thermalen Solen des Ruhrgebietes und ihre juvenilen Quellgase. *Glückauf*, *90*, 1334–1348, see also pages 1508–1519.

Pilger, A. (1961). Übersicht über die Gangvererzung des Ruhrgebietes. *Geologisches Jahrbuch, Beihefte*, *40*, 297–350.

Puchelt, H. (1964). Zur Geochemie des Grubenwassers im Ruhrgebiet. *Zeitschrift der deutschen geologischen Gesellschaft*, *116*, 167–203.

Rittenhouse, G. (1967). Bromine in oil-field waters and its use in determining possibilities of origin of these waters. *American Association of Petroleum Geologists Bulletin*, *51*, 2430–2440.

Rosenfeld, U. (1983). Beobachtungen und Gedanken zur Osning Tektonik. *Neues Jahrbuch der Geologie und Paläontologie Abhandlungen*, *166*, 34–49.

Schaeffer, R. (1983). Vererzungen in karbonischen und tertiären Sedimenten bei Velbert (Niederbergisches Land)—eine Zeitmarke für die saxonische Mineralisation des Rheinischen Schiefergebirges. *Zeitschrift der deutschen Geologischen Gesellschaft*, *134*, 225–245.

Schaeffer, R. (1984). *Die postvariszische Mineralisation im nordöstlichen Rheinsichen Schiefergebige*. Braunschweiger geologisch-paläontologische Dissertationen, 3, 206 pp.

Scherp, A., & Strübel, G. (1974). Zur barium–strontium-mineralisation. *Mineralium Deposita*, *9*, 155–168.

Solley, W. B. (1983). Estimated use of water in the United States. *United States Geological Survey Circular*, *1001*, 56.

Sonntag, C., Münnich, H. J., & Rozanski, K. (1983). Variations of deuterium and oxygen-18 in continental precipitation and groundwater, and their causes. In A. Street-Perrot, M. Beran, R. Ratcliffe (Eds.), *Variations in the global water budget* (pp. 107–124).

Struckmeier, W. (1990). Wasserhaushalt und hydrogeologische Systemanalyse des Münsterländer Beckens. *LWA (Landesamt für Wasser und Abfall Nordrhein-Westfalen) Schriftenreihe*, *45*, 72.

Stueber, A. M., Pushkar, P., & Hetherington, E. A. (1984). A strontium isotopic study of Smackover brines and associated solids, southern Arkansas. *Geochimica et Cosmochimica*, *48*, 1637–1649.

Sverjenski, D. A. (1984). Oil field brines as ore-forming solutions. *Economic Geology*, *79*, 23–37.

Thome, K. N. (1983). Gletschererosion und -akkumulation im Münsterland und angrenzenden Gebieten. *Neues Jahrbuch der Geologie und Paläontologie Abhandlungen*, *166*, 116–183.

Unland, G. (1985). Die Strontianitlagerstätte im Münsterland. *Aufschluss*, *36*, 371–374.

Wedepohl, K. H. (1978). *Handbook of geochemistry*, *Vol. II.* Berlin: Springer.

Wedewardt, M. (1995). Hydrochemie und Genese der Tiefenwässer im Ruhr-Revier. *DMT-Berichte aus Forschung und Entwicklung*, *39*, 250.

Wolansky, D. (1964). Die Hydrogeologie des Deckgebirges im niederrheinisch-westfälischen Revier in ihrer Bedeutung für den Bergbau. *Zeitschrift der deutschen geologischen Gesellschaft*, *116*, 55–69.

Zhou, X., & Li, C. (1992). Hydrogeochemistry of deep formation brines in the central Sichuan Basin, China. *Journal of Hydrology*, *138*, 1–15.